ELSEVIER

Journal of Fluids and Structures 20 (2005) 309–329

JOURNAL OF FLUIDS AND STRUCTURES

www.elsevier.nl/locate/jnlabr/yjfls

Numerical predictions of tuned liquid tank structural systems

J.B. Frandsen*

Department of Civil and Environmental Engineering, Louisiana State University, Baton Rouge, LA 70803, USA

Received 25 April 2004; accepted 2 August 2004

Abstract

A fully nonlinear 2-D σ-transformed finite difference solver has been developed based on inviscid flow equations in rectangular tanks. The fluid equations are coupled to a linear elastic support structure. Nonoverturning sloshing motions are simulated during structural vibration cycles at and outside resonance. The wave tank acts as a tuned liquid damper (TLD). The TLD response is highly nonlinear when large liquid sloshing occurs. The solver is valid at any water depth except for small depth when shallow water waves and viscous effects would become important. Results of liquid sloshing induced by horizontal base excitations are presented for small to steep nonbreaking waves at tank aspect ratios, depth to length, h/b of 0.5, 0.25 and 0.125, representing deep to near shallow water cases. The effectiveness of the TLD is discussed through predictions of coupling frequencies and response of the tank-structural system for different tank sizes and mass ratios between fluid and structure. An effective tank-structural system typically displays two distinct frequencies with reduced structural response (e.g., $h/b = 0.5$). These eigenfrequencies differ considerably from their noninteracting values. Hardening or softening spring behavior of the fluid, known to be present in solutions of pure sloshing motion in tanks, does not exists in the coupled system response. Strongest interactions occur with only one dominating sloshing mode when the nth sloshing frequency is close to the natural frequency of the structure, as the mass ratio between fluid and structure $\mu \to 0$. Inclusion of higher modes reduces the efficiency of the TLD. Good agreement is achieved between the numerical model and a first-order potential theory approximation outside the resonance region when the unsteady sloshing motions remain small. When the free-surface amplitudes become large in the coupled system, the numerical peaks are larger and the troughs become lower as time evolves (typical nonlinear effects) compared to the linear solution. Nonlinearities were found to reduce the system displacement significantly, e.g., system resonance shifted to beating response, compared to linear predictions. It was also found that the system response is extremely sensitive to small changes in forcing frequency. In conclusion, if strong interaction exists, the coupled system exhibits nonlinearity in structural and free-surface response, but the coupled eigenfrequencies compare well with the linear predictions. Furthermore, the solver removes the need for free-surface smoothing for the cases considered herein (maximum wave steepness of 1.2). The numerical model provides a quick and accurate way of determining system eigenfrequencies which can be hard to identify and interpret in physical experiments.

*Tel.: +1 225 578 0277; fax: +1 225 578 0245.
E-mail address: frandsen@lsu.edu (J.B. Frandsen).

0889-9746/$ - see front matter © 2004 Elsevier Ltd. All rights reserved.
doi:10.1016/j.jfluidstructs.2004.10.003

1. Introduction

For some large structures, structural damping alone has been insufficient to limit the dynamic motions to acceptable levels for serviceability considerations, as described in the review paper by Kareem et al. (1999). Thus, auxiliary dampers have been added. There exists a variety of different means of providing damping including the use of magnetorheological and electrorheological fluid dampers, as described by, e.g., Soong and Spencer (2002). Designers are faced with the task of understanding complex fluid–structure interaction when attempting to estimate energy dissipation performance of, for example, tuned sloshing dampers. To this end, numerical wave tank studies can provide useful information on the free-surface motions, resonant frequencies, etc., which can be hard to identify and interpret in physical experiments.

In this study, a 2-D rectangular numerical wave tank is coupled to an elastic support structure and acts as a tuned liquid damper (TLD). A TLD is tuned/designed to slosh at or near the natural frequency of the structure. When a structure with a TLD begins to sway due to external dynamic excitation, the fluid of the tank moves. The sloshing motion of the fluid modifies the global response of the structure resulting in a shift of the natural frequencies and a reduction of the structural displacements. The system response becomes highly nonlinear when the steepness of the free-surface grows. Approximate solutions cannot capture the nonlinearity at the free-surface accurately and thus the use of a fully nonlinear numerical model becomes advantageous in getting insight into TLD performance.

Traditionally, tuned mass dampers (TMD) have been used to suppress structural motion. From the theory of Den Hartog (1984), it is known that a TMD will only suppress structural motions at one frequency efficiently which makes this damping device less attractive when the load is associated with broad-banded spectra (e.g., wind, waves, earthquakes). In this case, TLDs are more attractive in the sense that they can be designed to suppress a range of unwanted frequencies. Other advantages of using TLDs are: easy adjustment of natural frequencies, low cost and maintenance, suitability for temporary use, etc. However, an adverse effect can occur if the wave motions do not diminish immediately after the cessation of the excitation, as some of the energy absorbed by the TLD is transferred back to the structure (Fujino et al., 1988). To mitigate this behavior, investigators have studied various options for improvement, for example, sloped bottom TLDs. This type of TLD was analyzed by Gardarsson et al. (2001) who studied sloshing motion in a tank with 30° sloped sides. This specific configuration resulted in softening the spring characteristic of the free-surface elevation due to nonlinear effects of wave runup onto the sloped surfaces.

TMDs are still the most commonly used devices in practice. However, innovative applications using liquid as a means of damping have been used in ship design and satellite stabilization (Abramson, 1966). Also, TLDs previously have also been used on offshore platforms (maybe not always intentionally), as described by, e.g., Vandiver and Mitone (1979) who developed an analytical TLD model. Also, water inside structural members of offshore platforms is another practical means of taking advantage of TLD behavior (e.g., the Chevron ALBA North Sea platform). Recently, water inside the single shaft of the 251 m deep Draugen gravity platform was used as a means of providing damping. Important studies were undertaken by Drake (1999) on sloshing interactions with multiple risers inside the shaft. These investigations were triggered by the occurrence of troublesome ringing excitation of the platform. Suppressing vibrations in towers or tall buildings due to along-wind or cross-wind forces are more recent examples where a TLD may prove to be an efficient type of vibration absorber.

Before reviewing work done on TLDs, it should be noted that the majority of investigations of predictions of sloshing motion in tanks have primarily been carried out without the coupling of the elastic structural support. Pure sloshing motion studies have been undertaken with fixed or prescribed base motions. The approaches used have involved experimental, theoretical and numerical work. Further details on sloshing studies are given in the extensive review by Ibrahim et al. (2001).

Approaches to the TLD problem have been principally experimental. Usually the system response in terms of structural displacements and associated system eigenfrequencies are reported. The literature does not reveal evidence on how the free surface behaves when coupled to the structure. The numerical fluid-structural solver presented herein is motivated by this fact. In order to explain the TLD performance, simultaneous coupled response of the free surface and structural response is emphasized.

TLD-structural model-scale experiments have been carried out by several investigators, e.g., Case et al. (2001), Vickery et al. (2001), etc. Some full-scale studies have also been undertaken, e.g., Fediw et al. (1993). Furthermore, important findings have been reported by Fujino et al. (1988) who identified that breaking surface waves are a major mechanism of energy dissipation compared to liquid viscosity and container bottom roughness. Sun and Fujino (1994) developed an analytical TLD model based on shallow water equations where wave breaking was accounted for through

a parameter derived from physical experiments. Most models are based on shallow water equations and most investigations are done on sloshing in rectangular tanks.

Some numerical TLD studies have been done using finite elements on moving grids based on the Arbitrary Lagrangian Eulerian formulation, e.g., Nomura (1994), Yamamoto and Kawahara (1999). Numerical instability problems at the free surface were reported by Yamamoto and Kawahara (1999) and their results included smoothing functions. Pure sloshing motion studies show that it is essential to describe the nonlinear free-surface behavior accurately in order to know if the TLD is working. Moreover, the free-surface motions are extremely sensitive to small changes in forcing frequency, e.g., Frandsen (2004). The ratios between fluid-to-structural mass, water depth and tank size are other important parameters in these studies.

This study presents a fully nonlinear coupled free-surface structural model. The fluid motion is described by nonlinear potential flow equations allowing steep nonoverturning waves to be captured. Two-dimensional solutions are obtained using a finite-difference time-stepping scheme on adaptively mapped grids. The fluid model is coupled to an elastic support structure, and extends the pure tank sloshing studies of Frandsen (2004). To the best knowledge of the author, this type of model has not been developed for investigations of TLD performance. The numerical model provides a quick and accurate way of determining system eigenfrequencies which can be hard to identify and interpret in physical experiments. In this study, sloshing motions are simulated during structural vibrations subjected to an external time-varying horizontal force. It should be noted that, if the tank size is large enough, the effects of viscosity and surface tension can be neglected and the energy dissipation will be caused by wave breaking only. As described, the fluid model herein applies to application of small to steep waves, which is desirable for many structural systems in which fatigue loading is of a concern. The solver is valid at any water depth, except for smaller depths when shallow water waves and viscous effects would become important. The effectiveness of the TLD is discussed through prediction of coupling frequencies and response of the tank-structural system for different tank sizes, mass ratio between fluid and structure and tuning ratio. The solver removes the need for free-surface smoothing for the cases considered herein.

2. Problem formulation

Investigations of the interaction between a generic horizontally excited structure and 2-D nonlinear motion of liquid in tanks are undertaken. Consider the system schematically shown on Fig. 1. A structure with mass $\hat{m}$, damping $\hat{c}$ and stiffness $\hat{k}$ has an attached 2-D rectangular water tank of width $\hat{b}$ and depth $\hat{h}$. Hats denote dimensional variables. The rectangular Cartesian coordinate system $(\hat{x},\hat{z})$ has its origin on the left wall of the tank with vertical $\hat{z}$-axis and $\hat{x}$-axis located on the undisturbed water level. The system is exposed to a unsteady horizontal force $\hat{F}(\hat{t})$. It is assumed that the fluid motion in the tank can be described by the Laplace equation for the velocity potential $\hat{\phi}$, together with no-flow boundary conditions on the rigid surfaces as well as dynamic and kinematic boundary conditions on the free water surface $\hat{z}=\hat{\zeta}(\hat{x},\hat{t})$.

First, the nondimensional variables are defined as

$$\begin{aligned}&(\hat{x},\hat{z})=\hat{L}(x,z), \quad \hat{\zeta}=\hat{a}\zeta, \quad \hat{X}=\hat{a}X,\\ &\hat{t}=(\hat{L}/\hat{g})^{1/2}t, \quad \hat{\phi}=\hat{a}(\hat{L}\hat{g})^{1/2}\phi,\end{aligned} \tag{2.1}$$

where $\hat{L}$ is the characteristic linear size of the problem (herein chosen as the tank width $\hat{b}$), $\hat{a}$ is the characteristic amplitude of the motion, $\hat{g}$ is the acceleration due to gravity and $\hat{X}(\hat{t})$ represents the motion of the coupled system.

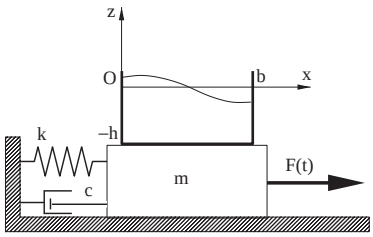

Fig. 1. The coupled system.

The problem formulation in non-dimensional form in a moving coordinate system (x, z) can now be written as

$$\begin{aligned}
&\nabla\phi = 0, \quad \frac{\partial\phi}{\partial x} = 0\bigg|_{x=0,b}, \quad \frac{\partial\phi}{\partial z} = 0\bigg|_{z=-h},\\
&\frac{\partial\zeta}{\partial t} - \frac{\partial\phi}{\partial z} + \varepsilon\frac{\partial\phi}{\partial x}\frac{\partial\zeta}{\partial x} = 0\bigg|_{z=\varepsilon\zeta},\\
&\frac{\partial\phi}{\partial t} = -\zeta - xX''(t) - \varepsilon\frac{1}{2}(\nabla\phi)^2\bigg|_{z=\varepsilon\zeta}.
\end{aligned} \tag{2.2}$$

There is an extra term in the surface dynamic condition due to the acceleration of the coordinate system, and $\varepsilon = \hat{a}/\hat{L}$. The horizontal acceleration of the tank $X''(t)$ is generated by the motion of the structure and is found from the equation of motion of the coupled system,

$$\hat{m}\hat{X}''(\hat{t}) + \hat{c}\hat{X}'(\hat{t}) + \hat{k}\hat{X}(\hat{t}) = \hat{F}(\hat{t}) + \hat{F}_I(\hat{t}),$$

where $\hat{F}_I(\hat{t})$ is the horizontal force component applied to the structure by the water in the tank. It can be found by integrating the pressure over the vertical tank walls,

$$\hat{F}_I(\hat{t}) = \int_{-\hat{h}}^{\hat{\zeta}(\hat{x},\hat{t})} \hat{p}(\hat{x},\hat{z},\hat{t})\,\mathrm{d}\hat{z}\bigg|_{\hat{x}=0}^{\hat{x}=\hat{b}}.$$

Introducing the nondimensional pressure and the internal force as follows, we have

$$\hat{p} = \hat{\rho}\hat{g}\hat{L}p, \quad \hat{F}_I = \hat{\rho}\hat{g}\hat{a}\hat{L}F_I,$$

where $\hat{\rho}$ is the liquid density. Using the unsteady Bernoulli equation,

$$\frac{\hat{p}}{\hat{\rho}} = -\hat{g}\hat{z} - \hat{x}\hat{X}''(\hat{t}) - \frac{\partial\hat{\phi}}{\partial\hat{t}} - \frac{1}{2}(\nabla\hat{\phi})^2,$$

the nondimensional internal force can be expressed in the following form:

$$F_I = \int_{-h}^{\varepsilon\zeta(x,t)} \left(\frac{\partial\phi}{\partial t} + \varepsilon\frac{1}{2}(\nabla\phi)^2\right)\mathrm{d}z\bigg|_{x=b}^{x=0} + \varepsilon\frac{1}{2}(\zeta(0,t)^2 - \zeta(b,t)^2) - (bh + \varepsilon\zeta(b,t))X''(t). \tag{2.3}$$

Next, introducing the characteristic amplitude of the external force $\hat{A}_F$: $\hat{F} = \hat{A}_F F$, the amplitude of the motion is $\hat{a} = \hat{A}_F/(\hat{\rho}\,\hat{g}\,\hat{L})$, and the nondimensional form of the equation of motion is

$$mX''(t) + cX'(t) + kX(t) = F(t) + F_I(t), \tag{2.4}$$

where the nondimensional mass, structural damping and stiffness are $m = \hat{m}/(\hat{\rho}\,\hat{L}^2)$; $c = \hat{c}/(\hat{\rho}\hat{g}^{1/2}\hat{L}^{3/2})$; $k = \hat{k}/(\hat{\rho}\hat{g}\hat{L})$. The internal force can be found by using Eq. (2.3). To complete the formulation, initial conditions are added to (2.2), (2.3) and (2.4). Initially the structure is assumed to be at rest and the water surface is undisturbed. The associated initial conditions are

$$\begin{aligned}
&\phi|_{t=0} = 0, \quad \zeta|_{t=0} = 0,\\
&X(0) = 0, \quad X'(0) = 0, \quad X''(0) = F(0)/m,
\end{aligned} \tag{2.5}$$

where the latter condition translates into zero internal force when the fluid is at rest and therefore only contains a contribution from the external force.

The parameter $\varepsilon = \hat{a}/\hat{L} = \hat{A}_F/(\hat{\rho}\hat{g}\hat{L}^2)$ is now recognized as a forcing parameter. Consider the limit of small forcing $\varepsilon \to 0$; applying this limit to (2.2)–(2.5), the following linear approximation for the velocity potential and system displacement $X(t)$ is found,

$$\begin{aligned}
&\nabla\phi = 0, \quad \frac{\partial\phi}{\partial x} = 0\bigg|_{x=0,b}, \quad \frac{\partial\phi}{\partial z} = 0\bigg|_{z=-h},\\
&\frac{\partial^2\phi}{\partial t^2} + \frac{\partial\phi}{\partial z}\bigg|_{z=0} = -xX'''(t),\\
&(m + bh)X''(t) + cX' + kX = F(t) + \int_{-h}^{0}\frac{\partial\phi}{\partial t}\,\mathrm{d}z\bigg|_{x=b}^{x=0}.
\end{aligned} \tag{2.6}$$

The first-order surface elevation can be found as

$$\zeta = -\left.\frac{\partial\zeta}{\partial t}\right|_{z=0} - xX''(t),$$

where (2.5) should be used as initial conditions.

3. Analytical model for linear tank–structure interaction

First, consider linearly behaved motion of the coupled system. The structure is herein represented as a one degree-of-freedom system (Fig. 1). The linear model describes approximate fluid sloshing motion in the tank, which can be used if the slope of the free surface $\partial\zeta/\partial x$ is small. The general dimensional linear solution for fluid motion in the rectangular tank can be written by using the natural modes of linear sloshing for the velocity potential,

$$\phi(x,z,t) = \sum_{n=1}^{\infty} \frac{\cosh(k_n(z+h))}{\cosh(k_n h)} \cos(k_n x)\Phi_n(t) \tag{3.1}$$

and surface elevation,

$$\zeta(x,t) = \sum_{n=1}^{\infty} \cos(k_n x) Z_n(t), \tag{3.2}$$

where the wave numbers are $k_n = \pi n/b$. The mean fluid level $z = 0$ is used to approximate the upper boundary of the fluid domain and the velocity potential is expressed via the surface elevation as $\partial\phi(x,0,t)/\partial z = \partial\zeta(t)/\partial t$. For the individual components, we have

$$\Phi_n(t) = \frac{g}{\omega_n^2} Z_n'(t),$$

where ω_n is the natural frequency of the nth sloshing mode, satisfying the linear dispersion relation $\omega_n^2 = gk_n \tanh(k_n h)$. Thus, the amplitudes of linear components of the surface elevation $Z_n(t)$ completely describe the linear motion of the fluid in the tank and can be used as a set of the generalized coordinates. For a coupled motion of the tank and the single degree-of-freedom structure, one more coordinate is introduced, which is the tank displacement with respect to the structural displacement $X(t)$. The kinetic energy of the system is

$$T = \frac{\rho}{2}\int_0^b \int_{-h}^0 \left(\left(\frac{\partial\phi}{\partial x} + X'(t)\right)^2 + \left(\frac{\partial\phi}{\partial z}\right)^2 \right) \mathrm{d}x\,\mathrm{d}z + \frac{m}{2} X'(t)^2 \tag{3.3}$$

and the potential energy of the system is

$$U = \rho g \int_0^b \int_{-h}^{\zeta} z\,\mathrm{d}x\,\mathrm{d}z + \frac{k}{2} X(t)^2, \tag{3.4}$$

taking into account the orthogonal properties of the sloshing modes. Using generalized coordinates yields

$$T = \frac{1}{2}(m + \rho bh)X'(t)^2 - 2\rho \sum_{n=1}^{\infty} \frac{\sin(\pi n/2)^2}{k_n^2} X'(t) Z_n'(t) + \frac{\rho g b}{4} \sum_{n=1}^{\infty} \frac{Z_n'(t)^2}{\omega_n^2}, \tag{3.5}$$

$$U = \frac{\rho g b}{4} \sum_{n=1}^{\infty} Z_n(t)^2 + \frac{k}{2} X(t)^2. \tag{3.6}$$

Now it is possible to construct the Lagrangian of the system in the form

$$L_s = T - U + W,$$

where $W = F(t)X(t)$ is the work of the external force F acting on the structure. The evolution of the n-th generalized coordinate is described by the Euler–Lagrange equations,

$$\frac{\partial}{\partial t}\frac{\partial L_s}{\partial \dot{u}_n} - \frac{\partial L_s}{\partial u_n} = 0.$$

The coupled system equations can be written in the following form:

$$\begin{aligned} &MX''(t) + cX'(t) + kX(t) - 2\rho \sum_{n=1}^{\infty} \frac{\sin(\pi n/2)^2}{k_n^2} Z_n''(t) = F(t), \\ &\frac{\rho g b}{2\omega_n^2} Z_n''(t) + \frac{\rho g b}{2} Z_n(t) - 2\rho \frac{\sin(\pi n/2)^2}{k_n^2} X''(t) = 0, \quad n = 1, 2 \ldots, \end{aligned} \tag{3.7}$$

where $M = m + \rho bh$ is the total mass of the system, i.e., m is the structural mass and ρbh represents the mass of the liquid. The coefficient $\sin(\pi n/2)^2 = 1$ for odd n and 0 for even n. This means that only odd (antisymmetric) modes interact with the structure.

Next, all functions are represented in the following nondimensional forms:

$$F(t) = A_F f(\omega t), \quad Z_n(t) = a(h/b) S_n(\omega_c t), \quad X(t) = a S_0(\omega_c t),$$

where A_F and ω are the amplitude and frequency of the external force, ω_c is a characteristic frequency, and $a = A_F/(M\omega_c)$ is the characteristic amplitude of the motion. Also, the nondimensional time $\tau = \omega_c t$ and the nondimensional frequencies $\Omega = \omega/\omega_c$ are introduced. Taking into account only the odd sloshing modes, the equations of motion become

$$\begin{aligned} &S_0''(\tau) - 2\mu \sum_{n=1}^{\infty} \frac{S_{2n-1}''(\tau)}{\pi^2(2n-1)^2} + \Omega_0^2 S_0(t) = f(\Omega\tau), \\ &S_n''(\tau) - 4R_n S_0''(\tau) + \Omega_n^2 S_n(\tau) = 0, \quad n = 1, 3, 5 \ldots, \end{aligned} \tag{3.8}$$

where $\mu = \rho bh/M$ is the mass ratio between fluid and structure, $\omega_0 = \sqrt{k/M}$ is the natural frequency of the structure with nonmoving liquid, $R_n = (\tanh(\pi nH))/(\pi nH)$, and $H = h/b$. Further, observe that the system behavior depends on a few nondimensional parameters: the mass ratio μ, the tank relative depth H, the structural natural frequency Ω_0, and the set of tank sloshing frequencies Ω_n. The nondimensional sloshing frequencies satisfy the following nondimensional dispersion relation $\Omega_n = \sqrt{\pi n \tanh(\pi nH)}/\mathrm{Fr}$, where $\mathrm{Fr} = \omega_c\sqrt{b/g}$ is the Froude number.

Some remarks about the system behavior can be made already from reading the terms of Eqs. (3.8). The first equation describes the motion of the structure with the natural frequency Ω_0 subjected to the external force f which is affected by the fluid motion in the tank. Each term of the sum represents the force applied to the structure by the nth tank sloshing mode. The equations describe the evolution of the individual sloshing modes with the natural frequencies Ω_n excited by the motion of the structure, as represented by the second term of each of these equations. These terms are proportional to the coefficients R_n, referred to as "receptivity coefficients" expressing the excitation sensitivity of each mode. The modes with higher receptivity are excited more easily by the structural motion. For a given tank geometry, the receptivity decreases for the higher modes. It should also be noted that R_n for each n grows as the relative depth H becomes smaller and reaches its maximum for $H \to 0$. The influence of the sloshing motion in the tank to the motion of the structure is proportional to the mass ratio μ and decreases as fast as $1/n^2$ for higher modes. Further, note that, if $\mu \to 0$, the second term of the first equation in (3.8) becomes negligible, which means that there is no interaction between the tank and the structure. The equation can then be integrated separately to estimate the structural motion $S_0(t)$. The second equation in (3.8) then describes the evolution of the sloshing modes in the tank moving with the prescribed horizontal acceleration $S_0''(t)$. The coupled natural frequencies for this noninteracting system are equal to the structural natural frequency Ω_0 and the tank sloshing frequencies Ω_n with small corrections of order of μ. However, if one of the sloshing frequencies is close to the natural frequency of the structure, then free structural oscillations will lead to an increase of the amplitude of the corresponding sloshing mode. Eventually, this mode will start to interact with the structure, which will result in a change of the natural frequencies of the coupled system. Thus, certain regions of resonant interaction exist where the strong interaction between the structure and one of the sloshing modes takes place even for small values of μ. The difference between the actual value of the natural frequency of the coupled system and its value for the corresponding noninteractingsystem can be used as a measure of the efficiency of the interaction. This will be discussed further in the next section, where the properties of the natural frequencies of the coupled tank-structural system are examined.

4. The natural frequencies and interaction efficiency of the coupled system

The frequencies of free oscillations of a linear system are the imaginary parts of the eigenvalues of the corresponding characteristic matrix of the system of Eqs. (3.8) given as

$$\mathbb{M} = \begin{pmatrix} \lambda^2 + \Omega_0^2 & -\mu\frac{2\lambda^2}{\pi^2 1^2} & -\mu\frac{2\lambda^2}{\pi^2 3^2} & \cdots \\ -4\lambda^2 R_1 & \lambda^2 + \Omega_1^2 & 0 & \cdots \\ -4\lambda^2 R_3 & 0 & \lambda^2 + \Omega_3^2 & \cdots \\ \vdots & \vdots & \vdots & \ddots \end{pmatrix},$$

and its eigenvalues λ can be found from

$$\det(\mathbb{M}) = (\lambda^2 + \Omega_0^2)\prod_{n_{\text{odd}}}(\lambda^2 + \Omega_n^2) - 8\mu\lambda^4 \sum_{n_{\text{odd}}} \frac{R_n}{\pi^2 n^2} \prod_{k_{\text{odd}} \neq n} (\lambda^2 + \Omega_k^2) = 0, \tag{4.1}$$

where the indexes take only odd values. Taking the limit as $\mu \to 0$, the asymptotic expansions for the eigenvalues are

$$\begin{aligned} \lambda_0^2 &= -\Omega_0^2 + 8\mu\Omega_0^4 \sum_{n_{\text{odd}}} \frac{R_n}{\pi^2 n^2(\Omega_n^2 - \Omega_0^2)} + \mathcal{O}(\mu^2), \\ \lambda_n^2 &= -\Omega_n^2 + \mu\frac{8\Omega_n^4 R_n}{\pi^2 n^2(\Omega_0^2 - \Omega_n^2)} + \mathcal{O}(\mu^2), \quad n = 1, 3, 5 \ldots . \end{aligned} \tag{4.2}$$

It can be observed that, in the case of small mass ratios, the eigenfrequencies of the system are equal to those of the uncoupled tank and the structure with small corrections of the order of μ due to the weak tank-structure interaction. Further, expansions (4.2) become nonuniformly valid when one of the tank sloshing frequencies approach the structural natural frequency (the corresponding term in the sum goes to infinity). Thus, strong interaction is assumed between the structural motion and this sloshing mode when one of the sloshing frequencies is close enough to the structural natural frequency. The corresponding eigenfrequencies in this case differ considerably from their noninteracting values.

Now, assume that the nth sloshing frequency is close to the natural frequency of the structure, that is, $\Omega_n^2 - \Omega_0^2 \to 0$ as $\mu \to 0$. For all other modes, the corresponding frequency difference is $\mathcal{O}(1)$ and the characteristic Eq. (4.1), can be divided by the product of $(\Omega_k^2 - \Omega_0^2)$; $k \neq n$, yielding

$$\left[(\lambda^2 + \Omega_0^2)(\lambda^2 + \Omega_n^2) - \mu\lambda^4\frac{8R_n}{\pi^2 n^2}\right] - 8\mu\lambda^4(\lambda^2 + \Omega_n^2)\sum_{k_{\text{odd}} \neq n} \frac{R_k}{\pi^2 k^2(\lambda^2 + \Omega_k^2)} = 0.$$

The terms in brackets correspond to the structure interaction with the nth tank sloshing mode, and the following term describes the influence of all other modes. If strong interaction between the structure and the nth sloshing mode exists, the two terms in the brackets should have the same order of magnitude. This is the case when $\lambda^2 - \Omega_0^2 \sim \lambda^2 - \Omega_n^2 \sim \sqrt{\mu}$ as $\mu \to 0$, which means that $\Omega_0^2 - \Omega_n^2 \sim \sqrt{\mu}$ in the interaction region. The magnitude of the term in the brackets, i.e., the measure of the interaction, has the order of $\sqrt{\mu}$. The next term $\mathcal{O}(\mu^{3/2})$ is much smaller. Thus, when the order of the magnitude of the difference between the square of the structural natural frequency and the square of the nth sloshing frequency becomes as small as $\sqrt{\mu}$, then a strong interaction between the corresponding modes takes place. The motion in this region is the motion of the structure coupled with the tank with only one dominating sloshing mode. The influence of all other tank sloshing modes is small. Taking into account all orders of magnitude discussed above, the characteristic equation inside the nth interaction region can be rewritten as

$$\left\{\lambda^2 + \left[\Omega_0^2 - 8\mu\Omega_0^4 \sum_{k_{\text{odd}} \neq n} \frac{R_k}{\pi^2 k^2(\Omega_0^2 + \Omega_k^2)} + \mathcal{O}(\mu^{3/2})\right]\right\}(\lambda^2 + \Omega_n^2) - \mu\lambda^4\frac{8R_n}{\pi^2 n^2} = 0.$$

The influence of noninteracting modes is equivalent to a small correction of the structural natural frequency. This can be taken into account by introducing an "effective" structural frequency $\tilde{\Omega}_0$ inside each of the interaction regions. The approximate formula to estimate the linear eigenvalues including mode interaction can be expressed as

$$\lambda_{0,n}^2 = -\frac{\pi^2 n^2(\tilde{\Omega}_0^2 + \Omega_n^2)}{2\pi^2 n^2 - 16\mu R_n} \pm \frac{\pi n\sqrt{\pi^2 n^2(\tilde{\Omega}_0^2 - \Omega_n^2)^2 + 32\mu R_n \tilde{\Omega}_0^2 \Omega_n^2}}{2\pi^2 n^2 - 16\mu R_n} + \mathcal{O}(\mu^{3/2}), \tag{4.3}$$

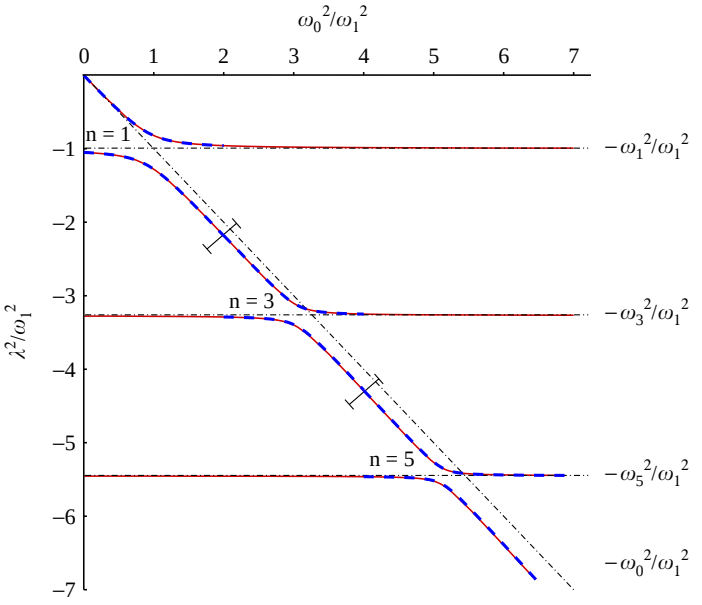

Fig. 2. Linear eigenvalues of the tank-structure system. The tank parameters are $\mu = 0.1$, $H = 1/2$, Fr $= 1$. The solid lines represent the exact solution (4.1). The approximate eigenvalues, calculated by Eq. (4.3) in the corresponding interaction region, are shown by dashed lines. The first sloshing frequency ω_1 is chosen as the characteristic frequency.

where the effective structural frequency inside the nth interaction region is

$$\tilde{\Omega}_0^2 = \Omega_0^2 - 8\mu\Omega_0^4 \sum_{k_{\text{odd}} \neq n} \frac{R_k}{\pi^2 k^2 (\Omega_0^2 + \Omega_k^2)}.$$

If weak interaction exists, Eqs. (4.2) can be used to estimate all other eigenvalues. Fig. 2 shows a very good agreement between the exact (from (4.1)) and the approximate eigenvalues (the example related to a mass ratio $\mu = 0.1$).

Although the present work builds on a potential solver and therefore strictly can only be used for frequency predictions, it is still important to estimate if the TLD would operate effectively. In the following, tank efficiency is discussed in relation to the strongest linear interaction between the tank and the structure. The strongest interaction takes place for the first sloshing mode, and the strength of the interaction decays fast ($1/n^2$) when n increases. Thus, the system should be tuned to work within the first interaction region. First, the tuning ratio $\Omega_1^T = \Omega_1/\Omega_0$ should be chosen from the condition of minimal difference between the two closest eigenfrequencies. From (4.3) it can be found that the difference $|\lambda_0| - |\lambda_1|$ has the minimal absolute value when

$$\Omega_1^T = 1 - \frac{4\mu}{\pi^2}\left(R_1 + \sum_{k_{\text{odd}} \neq 1} \frac{R_k}{\kappa_k^2 - 1}\right) + \mathcal{O}(\mu^2), \tag{4.4}$$

where $\kappa_n = \omega_n/\omega_1$. After specifying the tuning ratio, the parameter

$$E_{ff} = \frac{\min_{i \neq j}(|\lambda_i| - |\lambda_j|)^2}{\Omega_0^2}$$

is evaluated, which is a measure of the tank efficiency. The tank–structure interaction is more intensive for higher E_{ff}, and its value can be estimated by

$$E_{ff} = \frac{8\mu}{\pi^2}\left(R_1 - \sum_{k_{\text{odd}} \neq 1} \frac{R_k}{\kappa_k^2 - 1}\right) + \mathcal{O}(\mu^2), \tag{4.5}$$

where the first term in the bracket of (4.5) is due to the main interaction mode. The infinite sum accounts for small contributions from all other modes. As a first approximation, one can use the first term only (R_1). Thus, one can maximize the product $\mu \times R_1$. For a fixed mass ratio, μ this gives the maximum efficiency which is achieved for relatively small water depth (R_1 grows when $H = h/b$ decreases). This is still true when accounting for all other modes

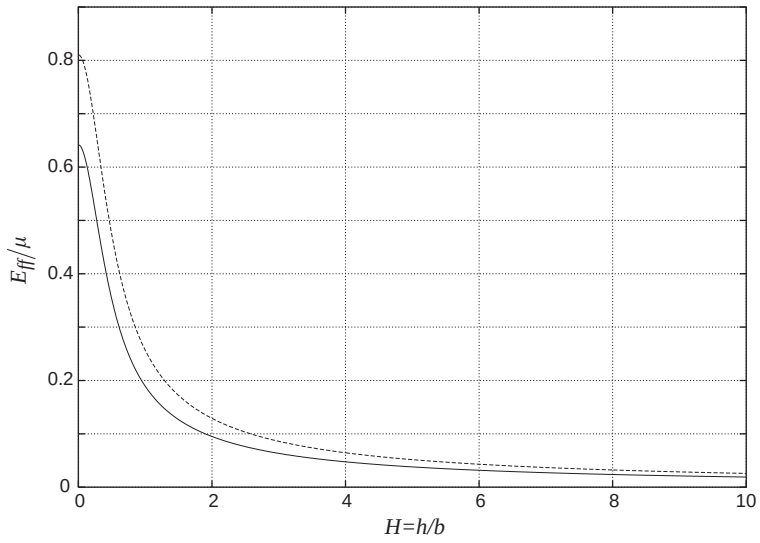

Fig. 3. Efficiency. – –, Mode 1 only; —, higher modes included.

but the efficiency reduces as these higher modes extract energy from the main most effective interaction (Fig. 3). In summary, in the context of TLD design, it becomes important to provide the tuning ratio, Eq. (4.4), and maximize the efficiency parameter, Eq. (4.5). The design process is usually restricted by fluid mass limitation and tank size. From a practical view point the E_{ff} parameter can be used as a guide but is not very informative because the tuning ratio vary for different tanks. The problem is, for a given structural frequency and choosing Ω_1^T, Eq. (4.4), one automatically selects the tank depth $H = h/b$. Therefore, there are not many parameters left for optimization.

Although the present paper does not involve the use of multiple tanks, it should be mentioned that multiple tanks can be designed to provide higher flexibility in the optimization process. The multiple tanks with identical geometric parameters can easily be taken into account by using the value $N\rho$ as a density, where N denotes number of tanks. The mass ratio is then $\mu = N\rho bh/M$. For a given mass ratio, the efficiency of a multiple tank-structural system is higher than the efficiency of a single tank system. For a given structure with prescribed mass ratio and structural stiffness ($\Omega_0 = \text{const}, \mu = \text{const}$), the tuning condition $\Omega_1 = \Omega_1^T \Omega_0$ leads to the following approximate relation between N and H: $\sqrt{NH}\tanh(\pi H) \approx \text{const}$. Thus, the value of H is smaller for a larger number of tanks N and, as a result, higher tank receptivity and higher value of the product μR_1 in (4.5) exist, and therefore higher efficiency. However, for a large number of tanks N, these arguments are not valid when H becomes too small, and viscous and nonlinear shallow water effects begin to play an important role. This is also true for a single tank.

For the reasons given above, optimum TLD-structural systems are herein discussed in terms of (1) shift in the system eigenfrequency ($\Delta\lambda_{\min} = |\lambda_0 - \lambda_n|$) relative to the structural natural frequency with nonmoving liquid, and (2) the reduction of the system response, X, due to the liquid sloshing. However, it should be mentioned that the performance of a TLD depends on its own inherent damping and would be necessary to estimate for optimal TLD performance. The literature does not offer any practical TLD rules; however, Luft (1979) and Den Hartog (1984) provide useful rules for optimum tuning and inherent damping values in relation to linear TMD performance.

5. Numerical model for nonlinear tank–structure interaction

This study presents a fully nonlinear coupled free-surface structural model. The fluid motion is described by nonlinear potential flow equations allowing steep nonoverturning waves to be captured. Two-dimensional solutions are obtained using a finite-difference time-stepping scheme on adaptively mapped grids. The fluid model is coupled to an elastic support structure, and extends the pure tank sloshing studies of Frandsen (2004). To the best knowledge of the author, this type of model has not been developed for investigations of TLD performance.

The sloshing standing waves are modeled applying a modified σ-transformation which is used to map the liquid domain onto a rectangle, such that the moving free surface in the physical plane becomes a fixed line in the mapped computational domain. The σ-transformation was first used by Phillips (1957) in connection with numerical weather

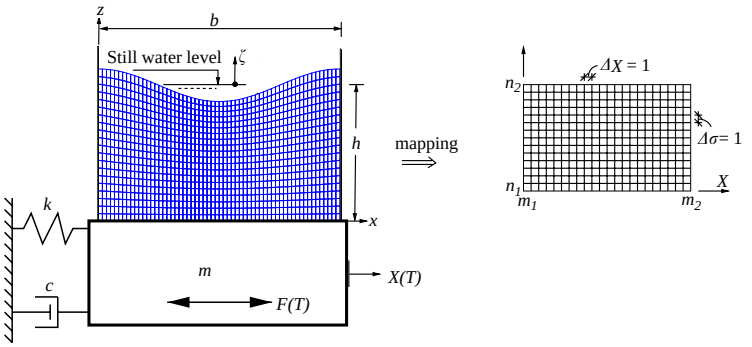

Fig. 4. The numerical model represented by a single degree-of-freedom structure coupled to a fluid tank. The physical fluid tank domain is mapped onto the computational domain.

forecasting schemes. Later the sigma coordinate system was used by Mellor and Blumberg (1985) for ocean modeling to improve predictions of instabilities in boundary layers. More recently Chern and Borthwick (1999) use a Chebyshev expansion to discretize the σ-transformed potential flow equation in their prediction of 2-D nonlinear free-surface motions. The latest model in the literature is described by Turnbull et al. (2003) who simulated inviscid free-surface wave motions using a σ-transformed 2-D finite element model.

Fig. 4 illustrates the effect of the mapping in the present tank–structural model. The fluid model has been designed so that each computational cell in the transformed domain is of unit size. This is the modified σ-transformation. In this model, remeshing due to the moving free-surface is avoided. Other advantages are that the mapping implicitly deals with the free-surface motion, and avoids the need to calculate the free-surface velocity components explicitly. Extrapolations are unnecessary, and so free-surface smoothing by means of a spatial filter is not required for the results presented here.

The following is the formulation in dimensional format. With reference to Fig. 4, the mappings from the physical (x, z, t) domain to the transformed (X, σ, t) domain are given by

$$x \longleftrightarrow X, \quad X = m_1 + \frac{(m_2 - m_1)}{b} x, \quad t \longleftrightarrow T, \quad T = t,$$

$$z \longleftrightarrow \sigma, \quad \sigma = n_1 + \frac{(n_2 - n_1)(z + h)}{H_t}, \tag{5.1}$$

where $H_t = \zeta + h$; the wave amplitude is ζ, the still water depth is h, and b is the tank width. The grid size spans from m_1 to m_2 in the horizontal x-direction and n_1 to n_2 in vertical z-direction.

The derivatives of the potential function $\phi(x, z, t)$ are transformed with respect to x, z and t into derivatives of $\Phi(X, \sigma, T)$.

The first derivatives of the velocity potential, ϕ, are obtained as

$$\frac{\partial \phi}{\partial x} = \frac{(m_2 - m_1)}{b}\left(\frac{\partial \Phi}{\partial X} + \frac{\alpha}{H_t}\frac{\partial \Phi}{\partial \sigma}\right),$$

$$\frac{\partial \phi}{\partial z} = \frac{(n_2 - n_1)}{H_t}\frac{\partial \Phi}{\partial \sigma}, \quad \frac{\partial \phi}{\partial t} = \frac{\partial \Phi}{\partial T} + \frac{\gamma}{H_t}\frac{\partial \Phi}{\partial \sigma}, \tag{5.2}$$

where $\alpha = -(\sigma - n_1)(\partial \zeta / \partial X)$ and $\gamma = -(\sigma - n_1)(\partial \zeta / \partial T)$.

Similarly, Laplace's equation can be rewritten as

$$\frac{\partial^2 \Phi}{\partial X^2} + \frac{1}{H_t}\left[\frac{\partial \alpha}{\partial X} - \frac{2\alpha}{H_t}\frac{\partial H_t}{\partial X}\right]\frac{\partial \Phi}{\partial \sigma} + 2\frac{\alpha}{H_t}\frac{\partial^2 \Phi}{\partial \sigma \partial X} + \left[\frac{\alpha^2}{H_t^2} + \frac{b^2(n_2 - n_1)^2}{H_t^2(m_2 - m_1)^2}\right]\frac{\partial^2 \Phi}{\partial \sigma^2} = 0. \tag{5.3}$$

The fixed vertical wall boundary condition on $X = m_1, m_2$ and the flat bed boundary condition on $\sigma = n_1$ become

$$\frac{\partial \Phi}{\partial X} = -\frac{\alpha}{H_t}\frac{\partial \Phi}{\partial \sigma}, \quad \frac{(n_2 - n_1)}{H_t}\frac{\partial \Phi}{\partial \sigma} = 0. \tag{5.4}$$

The kinematic free-surface boundary condition on $\sigma = n_2$ becomes

$$\frac{\partial \zeta}{\partial T} = \frac{(n_2 - n_1)}{H_t}\frac{\partial \Phi}{\partial \sigma}\left[1 + \frac{(m_2 - m_1)^2}{b^2}\left(\frac{\partial \zeta}{\partial X}\right)^2\right] - \frac{(m_2 - m_1)^2}{b^2}\frac{\partial \zeta}{\partial X}\frac{\partial \Phi}{\partial X}. \tag{5.5}$$

The dynamic free-surface boundary condition on $\sigma = n_2$ becomes

$$\frac{\partial \Phi}{\partial T} = \frac{(n_2 - n_1)}{H_t}\frac{\partial \zeta}{\partial T}\frac{\partial \Phi}{\partial \sigma} - \frac{1}{2}\left[\frac{(m_2 - m_1)^2}{b^2}\left(\frac{\partial \Phi}{\partial X} - \frac{(n_2 - n_1)}{H_t}\frac{\partial \zeta}{\partial X}\frac{\partial \Phi}{\partial \sigma}\right)^2 + \frac{(n_2 - n_1)^2}{H_t^2}\left(\frac{\partial \Phi}{\partial \sigma}\right)^2\right] - g\zeta - \left(\frac{X - m_1}{m_2 - m_1}\right)bX''(T), \tag{5.6}$$

where g denotes acceleration due to gravity and $X''(T)$ is the horizontal acceleration of the tank generated by the structural motion, given as

$$X''(T) = \frac{1}{m + \rho b H_t}[F(T) + F_I(T) - cX'(T) - kX(T))], \tag{5.7}$$

in which $F(T)$ is the external force and the internal force generated due to the sloshing motion is

$$F_I(T) = \frac{1}{2}\rho g(\zeta(0,T)^2 - \zeta(b,T)^2) + \rho\int_{\sigma=n_1}^{\sigma=n_2}\left[\frac{\partial \Phi}{\partial T} + \frac{\gamma}{H_t}\frac{\partial \Phi}{\partial \sigma} + \frac{1}{2}\left(\frac{(m_2 - m_1)}{b}\left(\frac{\partial \Phi}{\partial X} + \frac{\alpha}{H_t}\right)\right)^2 + \frac{1}{2}\left(\frac{(n_2 - n_1)}{H_t}\frac{\partial \Phi}{\partial \sigma}\right)^2\right]\frac{H_t}{n_2 - n_1}d\sigma\Big|_{X=m_1}^{X=m_2}. \tag{5.8}$$

Eqs. (5.3)–(5.6) are then discretized using the second-order Adams–Bashforth scheme and are solved in the transformed domain iteratively using successive over-relaxation.

6. Case studies

The linear structural and nonlinear fluid equations are solved simultaneously to predict free-surface motions and their effect on the frequencies of the coupled system for small to steep amplitude waves. Herein, the prescribed harmonic forced motion of $\hat{F}(\hat{t}) = \hat{A}_F\cos(\hat{\omega}\hat{t})$ where the dimensional parameter $\hat{A}_F$ denotes the horizontal forcing amplitude of the external force, $\hat{t}$ is time and $\hat{\omega}$ is the angular frequency of forced horizontal motion. Initially, the fluid in the tank and the structure is at rest and the initial acceleration at $\hat{t} = 0$ is due to the external force only. The system and the free-surface motions are numerically examined at resonance and off resonance.

The effect of the liquid sloshing on the structural motion is demonstrated by varying the tank size b/h, the fluid-to-structure mass ratio μ, and the tuning ratio relative to the structure $\Omega_n^T = \hat{\omega}_n/\hat{\omega}_0$ where $\hat{\omega}_0$ is the first natural structural frequency and $\hat{\omega}_n$ is the sloshing frequency of mode n. The free-surface behavior is investigated by varying the external forcing amplitude through the forcing parameter $\varepsilon = \hat{A}_F/(\hat{\rho}\hat{g}\hat{h}^2)$. As mentioned in Section 4, an optimum TLD-structural system is identified through the interaction efficiency with respect to (i) the shift in system eigenfrequency ($\Delta\lambda_{\min} = \mid \lambda_0 - \lambda_n \mid$) relative to the structural natural frequency with nonmoving liquid, and (ii) the reduction of the system response, X, due to the liquid sloshing. The fully nonlinear predictions are compared with the first-order potential flow structural solution, presented in Section 3. All results are presented in dimensionless format and hats denote dimensional parameters. The system displacements and free surface elevations are nondimensionalized by $(\hat{\rho}\hat{g}\hat{h})/\hat{A}_F$.The time histories of the forced sloshing motions are presented in nondimensional form using the first sloshing frequency ($\hat{\omega}_1$), so that the nondimensional time $\tau = \hat{\omega}_1\hat{t}$, and the nondimensional time step $\Delta\tau = \hat{\omega}_1\Delta\hat{t}$.

In the first test series, $b/h = 2$ and $\mu = 0.01$ and the tuning ratio $\Omega_1^T = 1$ are kept constant while the forcing amplitude is varied. A nondimensional time step of 0.011 and a grid size of 60×60 were used. Fig. 5 shows the free surface ζ and system displacement X time histories for small forcing amplitude ($\varepsilon = 0.0001$). Exact agreement between the numerical and first-order potential solution is found, as expected. In the test cases of Figs. 6 and 7, the forcing amplitude is increased both at and outside the resonance region where the forcing frequency ratio is defined as $\beta = \hat{\omega}/\hat{\omega}_0$. Outside the resonance region ($\beta = 0.67$), the numerical solutions with moderate and steep solutions ($\varepsilon = 0.102, 0.204$) agree well with the linear solution. At resonance ($\beta = 0.97$), the free-surface amplitudes grow as time evolves, the numerical peaks

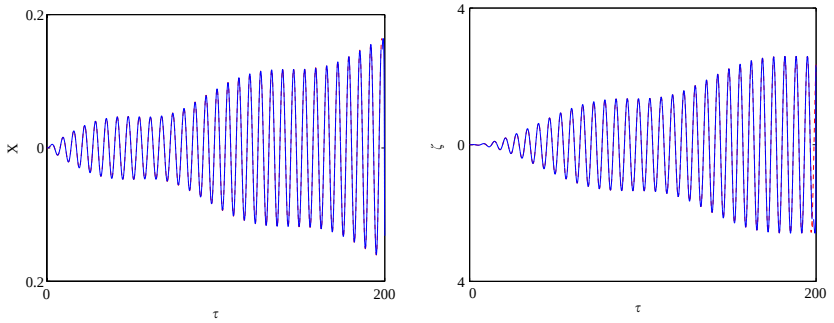

Fig. 5. System displacement, X, and free-surface elevation ($n = 1$) at the left wall, ζ. Resonance case ($\beta = 0.968$) for $\mu = 0.01$, $\Omega_1^T = 1$, $b/h = 2$, $\Delta\tau = 0.011$ and grid: 60×60. —, Numerical solution ($\varepsilon = 0.0001$); − −, linear solution.

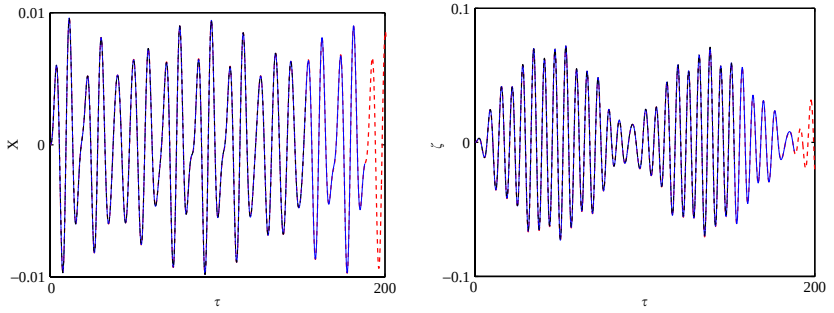

Fig. 6. System displacement, X, and free-surface elevation ($n = 1$) at the left wall, ζ. Off resonance case ($\beta = 0.665$) for $\mu = 0.01$, $\Omega_1^T = 1$, $b/h = 2$, $\Delta\tau = 0.011$ and grid: 60×60. − · −, Numerical solution ($\varepsilon = 0.204$); —, Numerical solution ($\varepsilon = 0.102$); − −, linear solution.

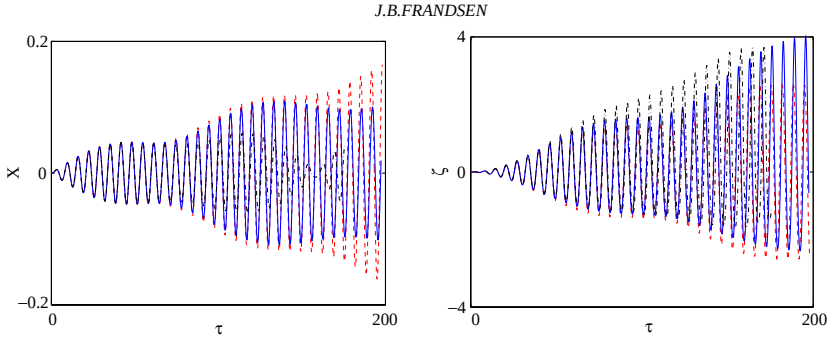

Fig. 7. System displacement, X, and free-surface elevation ($n = 1$) at the left wall, ζ. Resonance case ($\beta = 0.968$) for $\mu = 0.01$, $\Omega_1^T = 1$, $b/h = 2$, $\Delta\tau = 0.011$ and grid: 60×60. − · −, Numerical solution ($\varepsilon = 0.204$); —, Numerical solution ($\varepsilon = 0.102$); − −, linear solution.

are larger and the troughs become lower as time evolves compared to the linear solution (typical nonlinear effects). In the test cases involving $\varepsilon = 0.102, 0.204$, nonlinearities were found to reduce the system displacement significantly, e.g., system resonance shifted to beating response ($\varepsilon = 0.204$), compared to growing linear amplitude predictions. However, no shift in system frequencies was observed. Further, the wave steepness, defined as $S = k_n\hat{\zeta} = 1.2, 0.64$ (where $k_n = n\pi/\hat{b}$ is the wavenumber), respectively, versus the wave steepness of 0.0004 of the linear case. Also, this particular tank aspect ratio ($b/h = 2$) has a water depth above the critical water depth, defined as $\hat{h}_c/\hat{\lambda}_w = 0.162$ (Gu et al., 1988) where $\hat{\lambda}_w = 2\hat{b}/n$ denotes the wavelength. The $b/h = 2$ is a deep water case as $k_1\hat{h} > \pi/2$. Note in an uncoupled system the liquid is known to exhibit softening spring behavior whereas the coupled system shows increasing amplitudes with

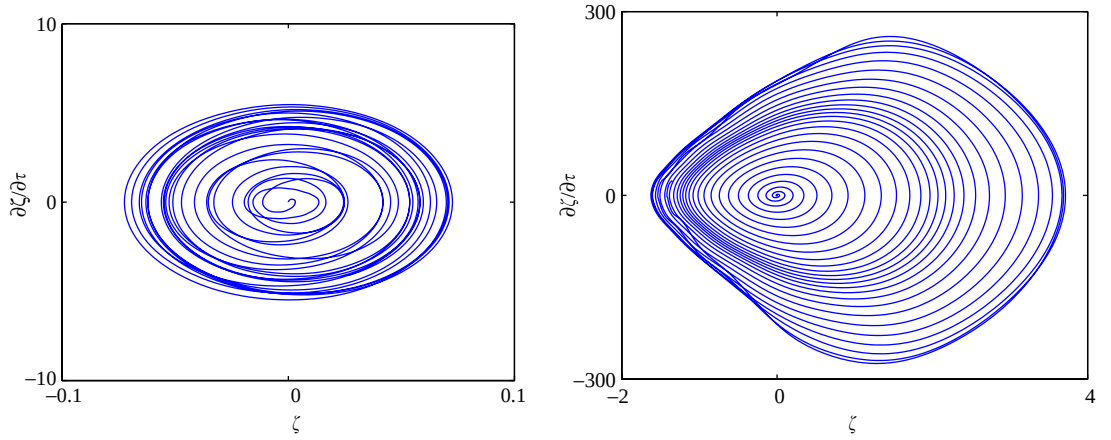

Fig. 8. Phase plane diagrams ($n = 1$) at left wall off resonance ($\beta = 0.665$) and at resonance ($\beta = 0.968$) for $\varepsilon = 0.204$, $\mu = 0.01$, $\Omega_1^T = 1$, $b/h = 2$, $\Delta\tau = 0.011$ and grid: 60×60.

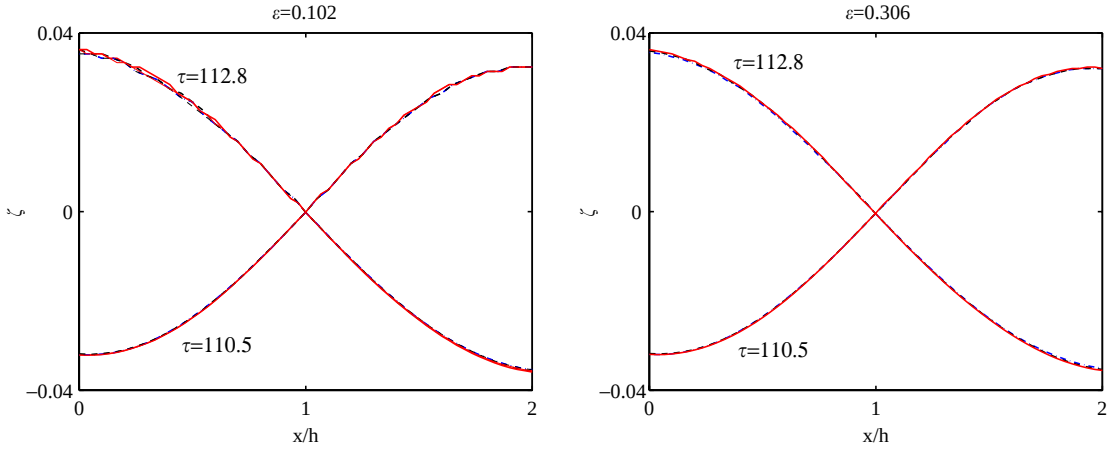

Fig. 9. Free-surface profiles ($n = 1$) outside resonance ($\beta = 0.665$) for $\mu = 0.01$, $\Omega_1^T = 1$ and $b/h = 2$ for $\Delta\tau = 0.011$ (dark curves) and $\Delta\tau = 0.006$ (light curves). Grid: $- \cdot -$, 40×40; $- \ -$, 40×60; —, 60×60.

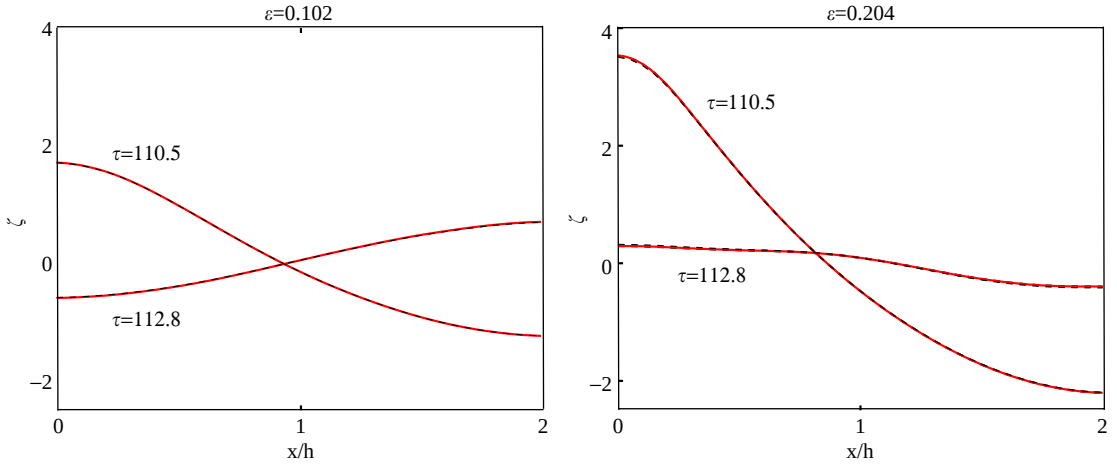

Fig. 10. Free-surface profiles ($n = 1$) at resonance ($\beta = 0.968$) for $\mu = 0.01$, $\Omega_1^T = 1$ and $b/h = 2$ for $\Delta\tau = 0.011$ (dark curves) and $\Delta\tau = 0.006$ (light curves). Grid: $- \cdot -$, 40×40; $- \ -$, 40×60; —, 60×60.

respect to linearly predicted frequencies (as discussed later, e.g., Fig. 11). Also *vice versa*, liquid behavior in shallow water ($k_n\hat{h}<\pi/10$) in an uncoupled system typically exhibits hardening spring behavior [e.g., Lepelletier and Raichlen (1988)], i.e., increasing amplitude with increasing frequency, that is, the maximum response is expected to occur at a higher frequency compared to the linear solution. The phase plane diagrams in Fig. 8 show more clearly the nonlinear solution at resonance for $\varepsilon = 0.204$ versus outside resonance behavior. The small amplitude wave phase-plane plot displays linear behavior of periodic beating in closed orbits with symmetry of peaks and troughs. The resonance case displays nonrepeatable nonclosed orbits in a stable system showing free-surface behavior typical of nonlinear systems. Note, that the velocity, $\partial\zeta/\partial\tau$, is nondimensionalized with $a_c\omega_1$ where $a_c = \hat{A}_F/(\hat{M}\hat{\omega}_1)$.

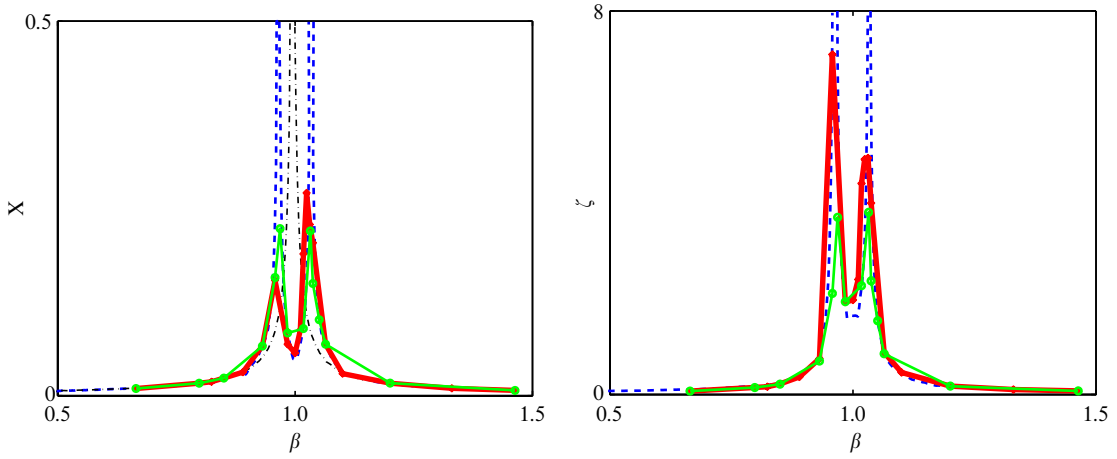

Fig. 11. System displacement, X, and free-surface elevation at the left wall, ζ, versus forcing frequency, β, for $\mu = 0.01$, $\Omega_1^T = 1$ and $b/h = 2$. —, numerical solution ($\varepsilon = 0.102$); ○-○, numerical solution ($\varepsilon = 0.0001$); − −, linear solution; − · −, structure with nonmoving liquid.

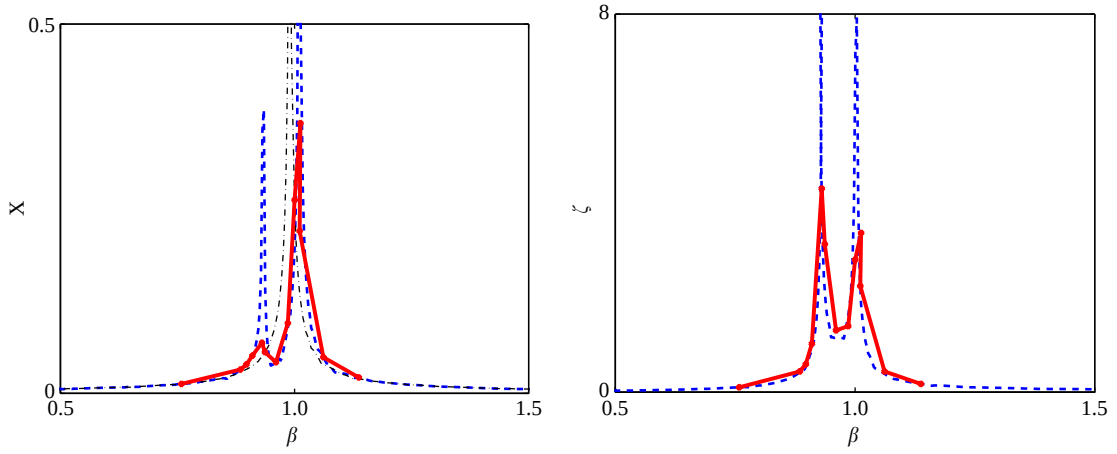

Fig. 12. System displacement, X, and free-surface elevation at the left wall, ζ, versus forcing frequency, β, for $\mu = 0.01$, $\varepsilon = 0.102$, $\Omega_1^T = 0.95$ and $b/h = 2$. —, numerical solution; − −, linear solution; − · −, structure with nonmoving liquid.

Table 1
Mass ratios and structural properties for $b/h = 2, 4, 8$ ($\hat{h} = 1$ m)

μ	0.005	0.01	0.02
M	402	202	102
k	579.03	290.96	146.92
c	1.25	0.63	0.32

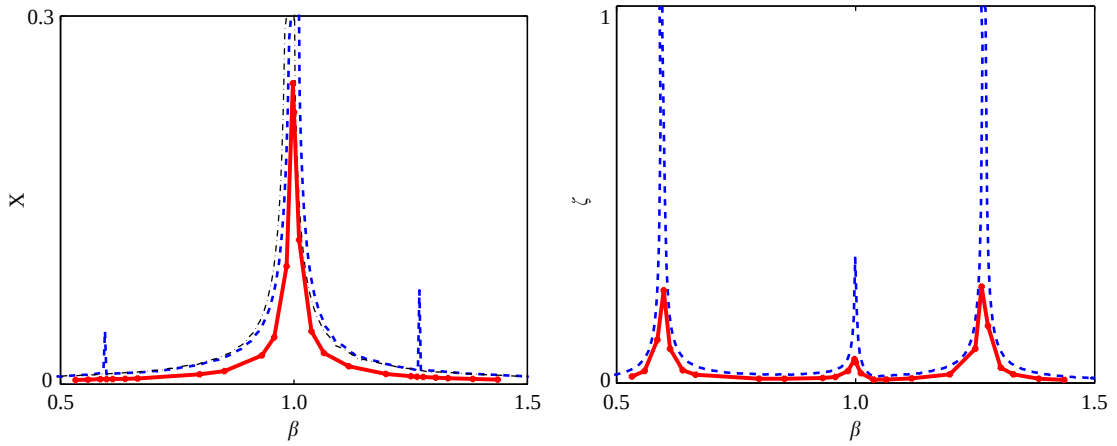

Fig. 13. System displacement, X, and free-surface elevation at the left wall, ζ, versus forcing frequency, β, for $\mu = 0.01$, $\varepsilon = 0.102$, $\Omega_1^T = 0.6$ and $b/h = 4$. —, numerical solution; – –, linear solution; – · –, structure with nonmoving liquid.

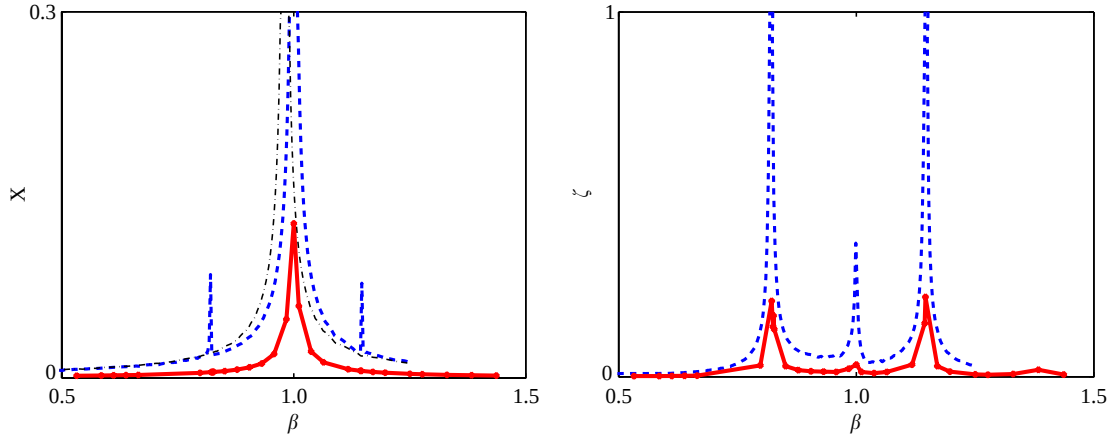

Fig. 14. System displacement, X, and free-surface elevation at the left wall, ζ, versus forcing frequency, β, for $\mu = 0.01$, $\varepsilon = 0.102$, $\Omega_1^T = 0.3$ and $b/h = 8$. —, numerical solution; – –, linear solution; – · –, structure with nonmoving liquid.

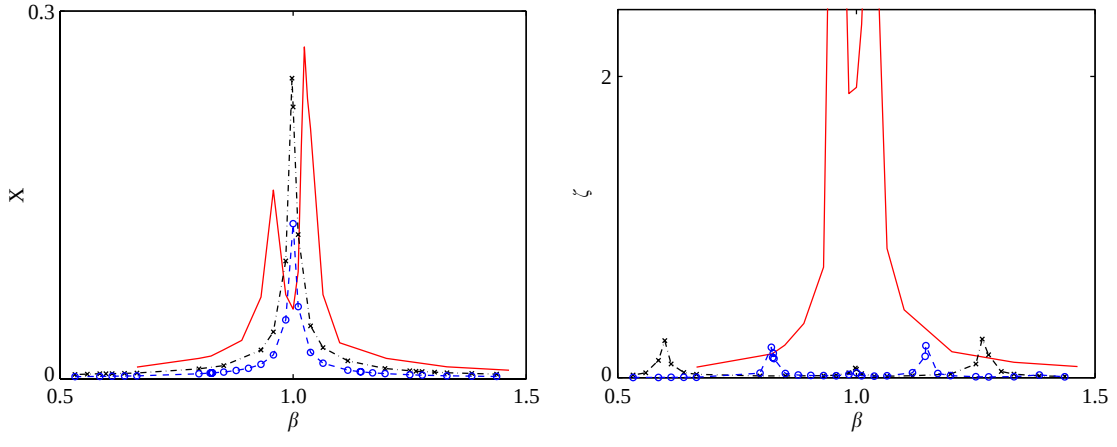

Fig. 15. Numerical solution. System displacement, X, and free-surface elevation at the left wall, ζ, versus forcing frequency, β, for $\mu = 0.01$ and $\varepsilon = 0.102$. —, $b/h = 2$ ($\Omega_1^T = 1$); · – × · –, $b/h = 4$ ($\Omega_1^T = 0.6$); – ○ –, $b/h = 8$ ($\Omega_1^T = 0.3$).

The next numerical tests carried out are designed to check the sensitivity of the numerical scheme to the time step, the grid resolution and associated nonlinear solutions. Figs. 9 and 10 show wave profiles along the tank at two different times for the first sloshing mode ($n = 1$) at and outside resonance. Results for different grid resolutions are shown related to moderate and steep wave amplitude ($\varepsilon \in [0.102, 0.306]$) for time steps of $\Delta\tau = 0.011$ and 0.006. Increasing the grid points in vertical direction was found to be more effective in improving accuracy than increasing the grid points in the horizontal direction. This was also found in the pure sloshing studies of Frandsen (2004). It was found that a grid size of 40×60 and a time step of 0.011 provided sufficient accuracy to capture nonlinearities related to steep wave predictions ($\varepsilon > 0.1$) outside resonance regions. At and near resonance the grid resolution needed to be increased to 60×60 and the time step reduced to 0.006.

In the second test series, $b/h = 2$ and $\mu = 0.01$ are kept constant while the tuning ratio Ω_1^T is varied relative to the first sloshing frequency ($\hat{\omega}_1$). In all outside resonance cases, a grid size of 60×60 and $\Delta\tau = 0.011$ were used whereas a time step of 0.006 was prescribed at and near resonance to maintain accuracy. Figs. 11 and 12 show the dimensionless amplitude response curves for the system (X) and for the free surface (ζ) as a function of the forcing frequency ratio β for $\Omega_1^T = 0.95, 1$. Note two distinct eigenfrequencies in the coupled system exist. For example the test case with $b/h = 2$ and $\Omega_1^T = 1$ (Fig. 11), displays eigenfrequencies $\lambda_1 = 0.97$ and $\lambda_3 = 1.03$. The largest sloshing motion exists at $\lambda_1 = 0.97$ and this motion results in maximum reduction of the structural response. This is also true at the second system frequency $\lambda_3 = 1.03$, but the reduction of the response at the higher mode is less, as expected. In general, good agreement in system eigenfrequencies is found between the fully nonlinear and first-order solution. As mentioned, the

Table 2
System eigenfrequencies for $\mu = 0.01$ and $b/h = 2, 4, 8$ ($\hat{h} = 1$ m)

b/h	2	4	8
Ω_1^T	1	0.6	0.3
Fr	1.7	1.4	1.0
R_1	0.58	0.83	0.95
λ_1	0.968	0.598	0.826
λ_3	1.031	1.0	1.0
λ_5	—	1.266	1.146
$\Omega_0^2 - \Omega_1^2$	0	1.8	10.0
E_{ff}^1/μ	0.47	0.67	0.77

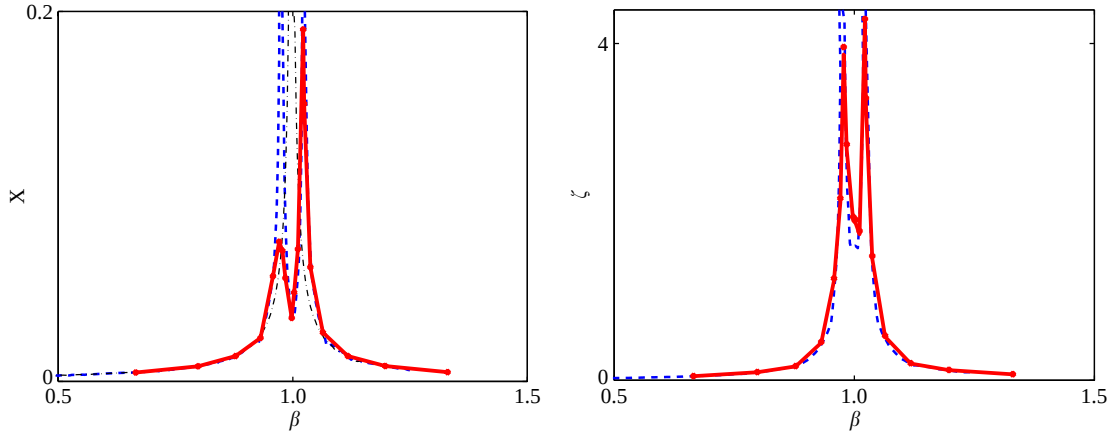

Fig. 16. System displacement, X, and free-surface elevation at the left wall, ζ, versus forcing frequency, β, for $\varepsilon = 0.102$, $b/h = 2$, $\Omega_1^T = 1$ and $\mu = 0.005$. —, numerical solution; – –, linear solution; – · –, structure with nonmoving liquid.

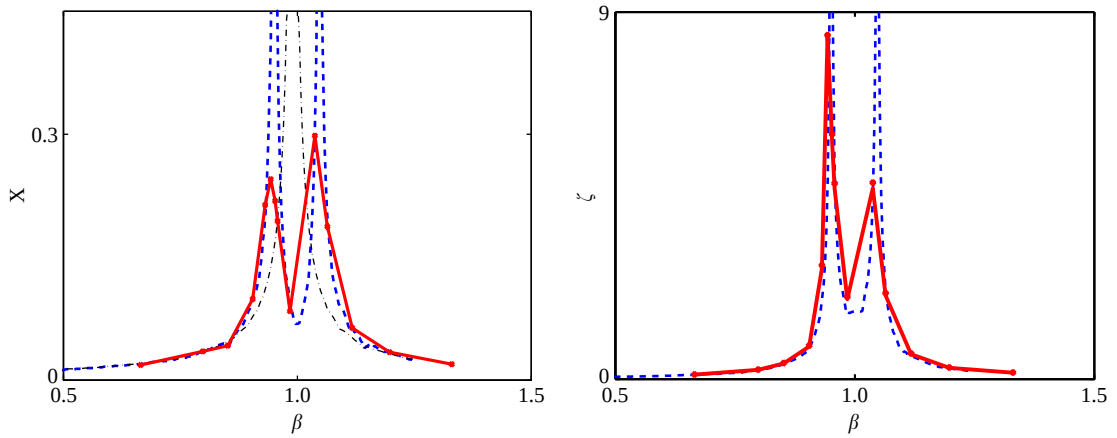

Fig. 17. System displacement, X, and free-surface elevation at the left wall, ζ, versus forcing frequency, β, for $\varepsilon = 0.102$, $b/h = 2$, $\Omega_1^T = 1$ and $\mu = 0.02$. —, numerical solution; – –, linear solution; – · –, structure with nonmoving liquid.

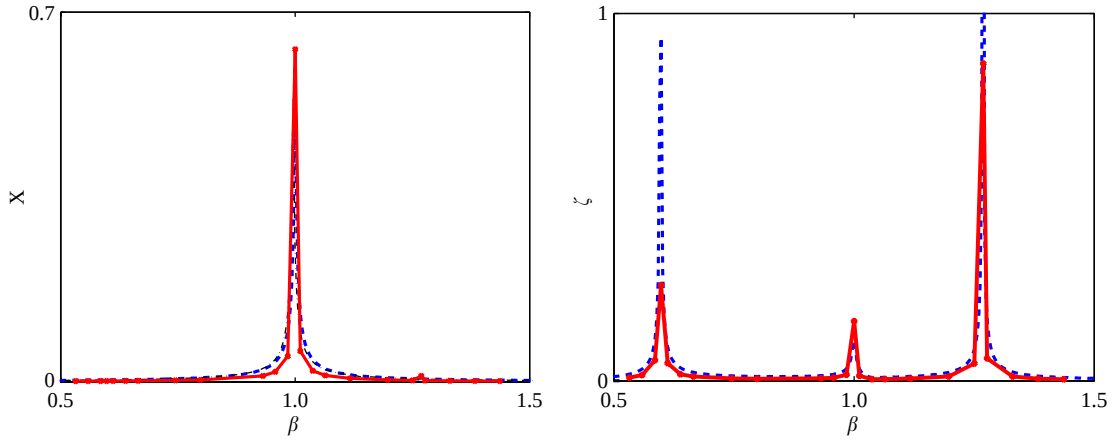

Fig. 18. System displacement, X, and free-surface elevation at the left wall, ζ, versus forcing frequency, β, for $\varepsilon = 0.102$, $b/h = 4$, $\Omega_1^T = 0.6$ and $\mu = 0.005$. —, numerical solution; – –, linear solution; – · –, structure with nonmoving liquid.

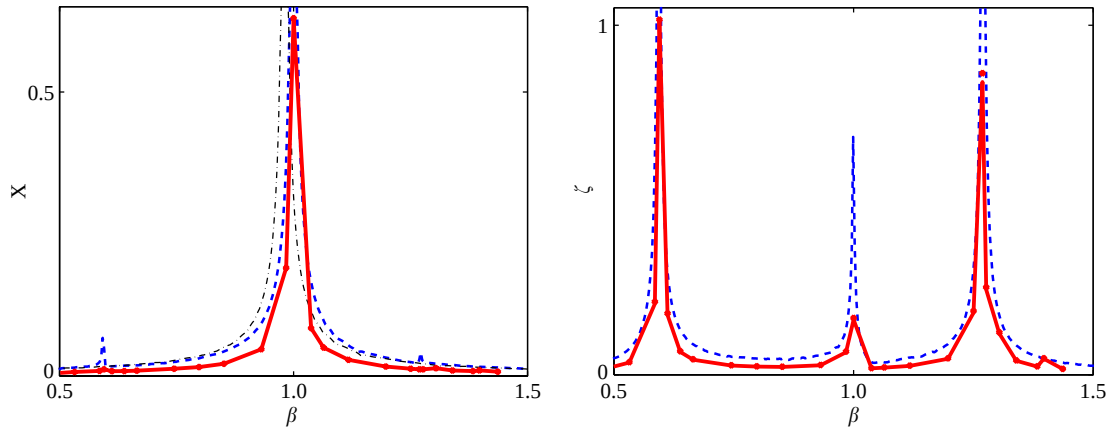

Fig. 19. System displacement, X, and free-surface elevation at the left wall, ζ, versus forcing frequency, β, for $\varepsilon = 0.102$, $b/h = 4$, $\Omega_1^T = 0.6$ and $\mu = 0.02$. —, numerical solution; – –, linear solution; – · –, structure with nonmoving liquid.

current nonlinear solver cannot simulate overturning waves and therefore the importance of wave breaking effects on system frequencies is not discussed herein. In the test series where $\Omega_1^T = 1$ (Fig. 11), the forcing parameter $\varepsilon \in [0.0001, 0.204]$ is also varied to demonstrate the effect of nonlinear free-surface motion on system behavior. The large sloshing motion with $\varepsilon = 0.102$ and 0.204 results in a decrease in system displacement compared to the linear solution which exhibits growing amplitudes in time (see also Fig. 7)and has equal magnitude displacements at each of the eigenfrequencies. In other words, the solution of the linear system displacement is overpredicted due to underpredicted free surface elevations at and near λ_1. This is also the case for $\Omega_1^T = 0.95$ (Fig. 12). However, note that the $\Omega_1^T = 1$ test (Fig. 11) has a maximum displacement smaller than the maximum displacement of the $\Omega_1^T = 0.95$ case, although $\Delta\lambda_{\min}$ is smaller compared to $\Omega_1^T = 1$. Therefore, the $\Omega_1^T = 1$ case is more efficient due to larger sloshing motions.

In the third test series, the fluid-to-structure mass ratio $\mu = 0.01$ and the forcing parameter $\varepsilon = 0.102$ are kept constant while the tank size is varied ($b/h = 4, 8$ where $\hat{h} = 1$ m). These tank aspect ratios relate to intermediate ($\pi/10 < k_1\hat{h} = 0.79 < \pi/2$) and near shallow water ($k_1\hat{h} = 0.39$) cases. The dimensionless parameters of the case studies are listed in Table 1. A grid size of 60×60 and $\Delta\tau = 0.011$ were used in all cases of the third test series. Figs. 13 and 14 show the dimensionless amplitude response curves of the system displacement (X) and the free-surface elevation (ζ) as a function of the forcing frequency ratio β. For these tank aspect ratios, the sloshing motion has negligible effect on the structural response. In general, there is good agreement between the numerical and first-order eigenfrequencies. The first-order solution displays similar fluid–structure interaction effects as the fully nonlinear model for forcing $\varepsilon < 0.102$. As mentioned, the strongest interaction effect is found when $\hat{\omega}_1$ is closest to $\hat{\omega}_0$. It can be observed that the $b/h = 4, 8$

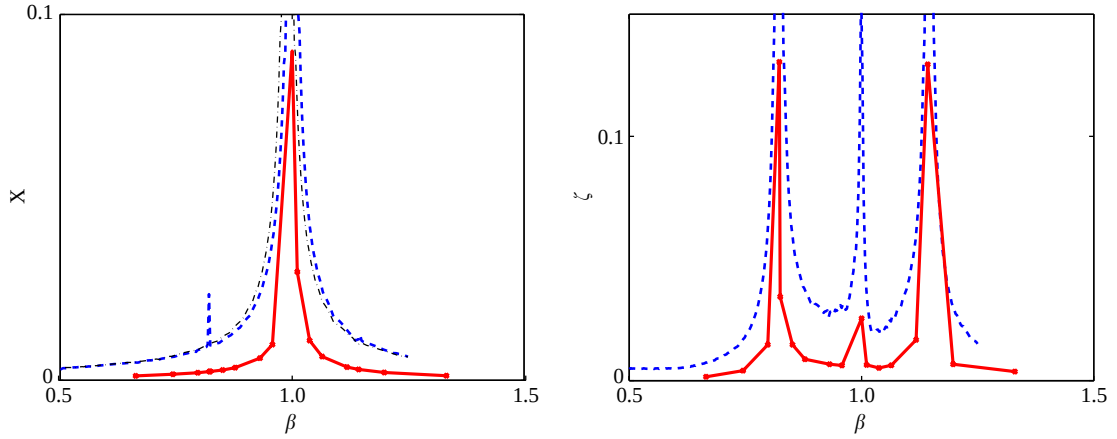

Fig. 20. System displacement, X, and free-surface elevation at the left wall, ζ, versus forcing frequency, β, for $\varepsilon = 0.102$, $b/h = 8$, $\Omega_1^T = 0.3$ and $\mu = 0.005$. —, numerical solution; − −, linear solution; − · −, structure with nonmoving liquid.

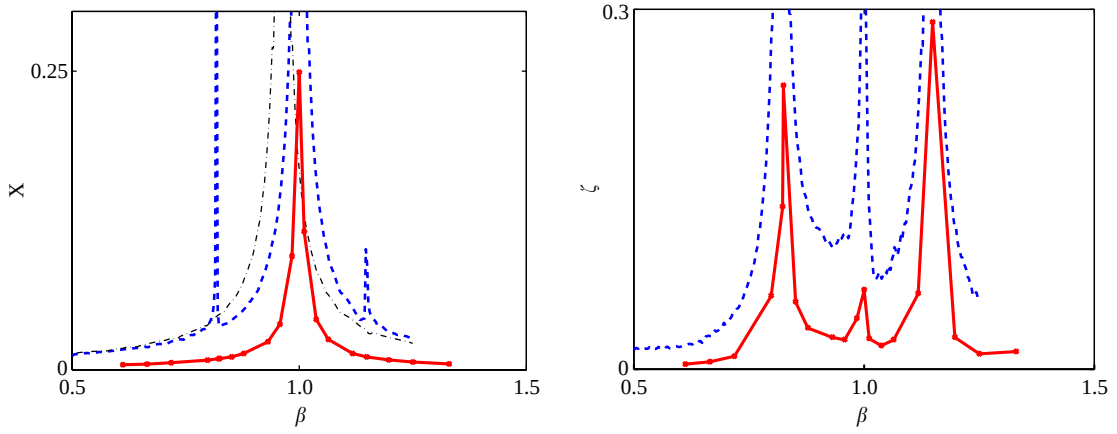

Fig. 21. System displacement, X, and free-surface elevation at the left wall, ζ, versus forcing frequency, β, for $\varepsilon = 0.102$, $b/h = 8$, $\Omega_1^T = 0.3$ and $\mu = 0.02$. —, numerical solution; − −, linear solution; − · −, structure with nonmoving liquid.

cases do not exhibit strong interaction as the eigenfrequencies are too far from the eigenfrequency of the structure (with nonmoving liquid). In other words, there is simply not enough energy in the sloshing motion to shift the system frequency. As a result, we therefore have one distinct frequency of the coupled system. This is also clearly demonstrated in Fig. 15 which shows the $b/h = 4, 8$ response casesrelative to the stronger interaction test case of $b/h = 2$. The associated system eigenfrequencies are listed in Table 2. The efficiency parameter (4.5) has also been estimated (based on the first mode only). It is largest for $b/h = 8$. However, the tuning ratio is also furthest away from the first natural frequency of the structure and, as a result, is not the optimum solution. Furthermore, it should be noted that changing the tank width means that the sloshing frequency of the water changes simultaneously. The natural frequency of the structure was kept constant. Choosing different structures should of course be done in the process of identifying an optimum coupled system. This would also provide an improved insight into the b/h parameter effects on the TLD performance. However, the structure in these studies has a natural frequency of 0.6 Hz and represents well a generic slender structure.

In the fourth test series, the mass ratio is varied. Figs. 16–21 show the response curves for $\mu = 0.005, 0.02$ for the tank sizes $b/h = 2, 4, 8$. System eigenfrequencies were similar to those listed in Table 2. Also similar findings were observed compared to $\mu = 0.01$ for $b/h = 2, 4, 8$. The tank size of $b/h = 2$ still displays the strongest interaction effects ($\Delta\lambda_{\min} = 0.03$) with $b/h = 4, 8$ showing negligible effects ($\Delta\lambda_{\min} = 0.40, 0.17$). But more water ($\mu = 0.02$) does help in increasing efficiency of the fluid-structure interaction, as expected. This can also be observed when comparing Figs. 22 and 23 which show direct comparisons between b/h and μ.

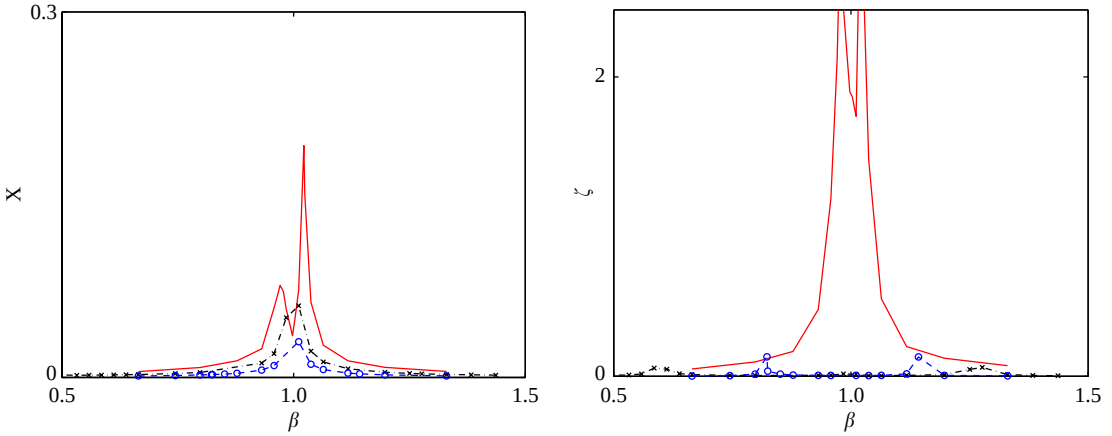

Fig. 22. Numerical solution. System displacement, X, and free-surface elevation at the left wall, ζ, versus forcing frequency, β, for $\mu = 0.005$ and $\varepsilon = 0.102$. —, $b/h = 2$ ($\Omega_1^T = 1$); · − × · −, $b/h = 4$ ($\Omega_1^T = 0.6$); − ○ −, $b/h = 8$ ($\Omega_1^T = 0.3$).

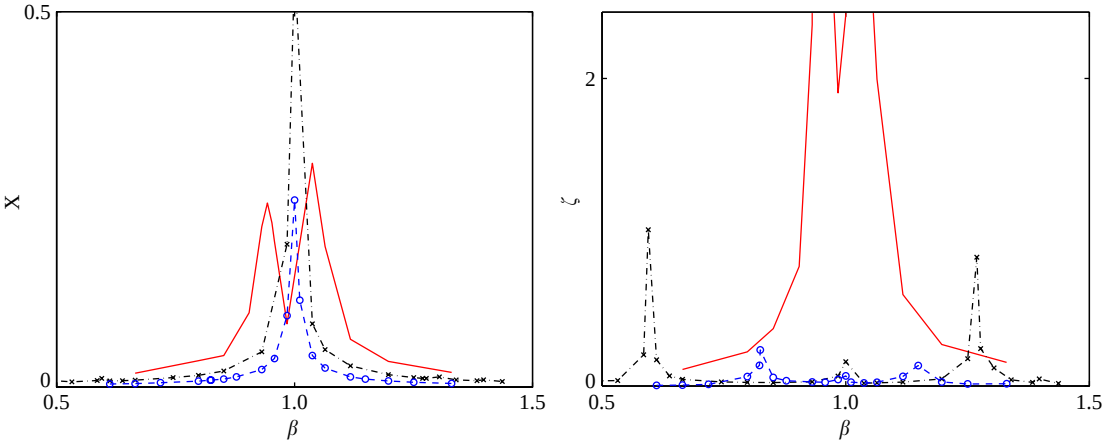

Fig. 23. Numerical solution. System displacement, X, and free-surface elevation at the left wall, ζ, versus forcing frequency, β, for $\mu = 0.02$ and $\varepsilon = 0.102$. —, $b/h = 2$ ($\Omega_1^T = 1$); · − × · −, $b/h = 4$ ($\Omega_1^T = 0.6$); − ○ −, $b/h = 8$ ($\Omega_1^T = 0.3$).

Finally, the numerical data point of the response curves (Figs. 11–23) at and near resonance represents maximum values based on the $\tau = 750$ time series, and outside resonance approximate $\tau = 190$ time series. Resonance points took an average of 36 hours on a single Pentium 3 GHz processor whereas the data point outside resonance were generated during 12 h real time.

7. Conclusions

The numerical predictions showed that the coupling of a liquid storage tank to a structure can change the behavior of the structure considerably. Conversely, the structural movements also affect the motion of liquid. Optimum TLD-structural systems are herein discussed in terms of (i) shift in system eigenfrequency of the dominating sloshing mode relative to the structural natural frequency with nonmoving liquid, and (ii) the reduction of the system response, X, due to the liquid sloshing. However, it should be mentioned that the performance of a TLD also depends on its own inherent damping and would be necessary to estimate for optimal TLD performance. This paper does not include a discussion on the damping contribution of the liquid nor the effects of wave breaking due to limitation of the potential flow solver.

Typically, an effective tank-structural system (e.g., $h/b = 0.5$) displayed two distinct frequencies on the system displacement curves with reduced response, especially at the first system eigenfrequency, due to large sloshing motion. The coupled system behaved in an optimized manner with regard to structural response reduction when one dominating sloshing frequency was near the structural frequency. The influence of the tank sloshing motion of mode n to the structural motion is proportional to the mass ratio between fluid and structure and decreases with $1/n^2$ for higher modes. Inclusion of higher modes reduces the efficiency of the TLD. The eigenfrequencies differ considerably from their noninteracting values. The hardening or softening spring behavior of the fluid, known to be present in solutions of pure sloshing motion in tanks, does not exists in the coupled system response.

The parametric studies in which tank aspect ratio, h/b (deep to near shallow water), fluid-to-structural mass and tuning ratio, were varied showed good agreement between numerical and linear solutions for forcing amplitude ($\varepsilon < 0.1$). For large sloshing motions ($\varepsilon > 0.1$) and in the case of strong interaction ($h/b = 0.5$), the coupled natural frequencies predicted by the linear and nonlinear model agreed well for small to steep waves. However, the linearly predicted system displacements were overpredicted due to the under-estimated free-surface elevations compared to the fully nonlinear predictions. Therefore, the linear solution should only be used for predicting system eigenfrequencies. The linear solution of the free surface is accurately predicting the structural and free-surface responses outside resonance when the sloshing amplitudes are small. If strong interaction exists, large amplitude sloshing solutions are generated and the fully nonlinear solution should be used for the evaluation of the TLD performance.

The numerical simulations presented provide indications that the σ-transformed finite difference solver can give helpful insight into TLD–structure interactions. Furthermore, nonlinear free-surface behavior plays an important role in describing the performance of TLDs accurately. The present studies can easily be expanded to include multiple wave tanks to investigate tank interaction effects, and thus cover suppression of a wider range of frequencies.

Acknowledgements

I am very grateful to Prof. C. Dalton, Department of Mechanical Engineering, University of Houston, for the many valuable comments to the manuscript.

References

Abramson, H.N., 1966. The dynamics of liquids in moving containers. Rep. SP 106. NASA.

Case, P.C., Tait, M., Isyumov, N., 2001. Tuned liquid dampers for the high cliff building, Hong Kong. Technical Report BLWT-SS8-2001. The Boundary Layer Wind Tunnel, The University of Western Ontario, London, Ont., Canada.

Chern, M.J., Borthwick, A.G.L., Eatock Taylor, 1999. A pseudospectral σ-transformation model of 2-D nonlinear waves. Journal of Fluids and Structures 13, 607–630.

Den Hartog, J.P., 1984. Mechanical Vibrations. Dover Publications, New York.

Drake, K.R., 1999. The effect of internal pipes on the fundamental frequency of liquid sloshing in a circular tank. Applied Ocean Research 21, 133–143.

Fediw, A.A., Breukelman, B., Morrish, D.P., Isyumov, N., 1993. Effectiveness of a tuned sloshing water damper to reduce the wind-induced response of tall buildings. Proceedings of the 9th US Conference on Wind Engineering. Los Angeles, CA, USA.

Frandsen, J.B., 2004. Sloshing motion in excited tank. Journal of Computational Physics 196, 53–87.

Fujino, Y., Pacheco, B.M., Chaiseri, P., Sun, L.M., 1988. Parametric studies on tuned liquid damper (tld) using circular containers by free-oscillation experiments. JSCE Journal of Structural Engineering/Earthquake Engineering 5, 381–391.

Gardarsson, S., Yeh, H., Reed, D., 2001. Behavior of sloped-bottom tuned liquid dampers. ASCE Journal of Engineering Mechanics 127, 266–271.

Gu, X.M., Sethna, P.R., Narain, A., 1988. On three-dimensional nonlinear subharmonic resonance surface waves in a fluid: part I-Theory. Journal Applied Mechanics 55, 213–219.

Ibrahim, R.A., Pilipchuk, V.N., Ikeda, T., 2001. Recent advances in liquid sloshing dynamics. ASME Applied Mechanics Reviews 54, 133–199.

Kareem, A., Kijewski, T., Tamura, Y., 1999. Mitigation of motions of tall buildings with specific examples of recent applications. Journal of Wind and Structures 2, 201–251.

Lepelletier, T.G., Raichlen, F., 1988. Nonlinear oscillations in rectangular tanks. ASCE Journal of Engineering Mechanics 114, 1–23.

Luft, R.W., 1979. Optimal tuned mass dampers for buildings. ASCE Journal of the Structural Division 105, 2766–2772.

Mellor, G.L., Blumberg, A.F., 1985. Modelling vertical and horizontal diffusivities with the sigma transform system. Applied Ocean Research 113, 1379–1383.

Nomura, T., 1994. ALE finite element computations of fluid–structure interaction problems. Computer Methods in Applied Mechanics and Engineering 112, 291–308.

Phillips, N.A., 1957. A coordinate system having some special advantages for numerical forecasting. Journal of Meteorology 14, 184–185.

Soong, T.T., Spencer Jr., B.F., 2002. Supplemental energy dissipation: state-of-the-art and state-of-the-practice. Engineering Structures 24, 243–259.

Sun, L.M., Fujino, Y., 1994. A semi-analytical model for tuned liquid damper (tld) with wave breaking. Journal of Fluids and Structures 8, 471–488.

Turnbull, M.S., Borthwick, A.G.L., Eatock Taylor, R., 2003. Numerical wave tank based on a σ-transformed finite element inviscid flow solver. International Journal for Numerical Methods in Fluids 42, 641–663.

Vandiver, J.K., Mitone, S., 1979. The effect of liquid storage tanks on the dynamic response of offshore platforms. Journal of Petroleum Technology 31 (10), 1231–1240.

Vickery, B.J., Galsworthy, J.K., Gerges, R., 2001. The behaviour of simple non-linear tuned mass dampers. Proceedings 6th World Congress of the Council on Tall Buildings and Urban Habitat. Melbourne, Australia.

Yamamoto, K., Kawahara, M., 1999. Structural oscillation control using tuned liquid dampers. Computers and Structures 71, 435–446.